Luminescence R-line spectrum of ruby crystals shocked to 125 kbar along the crystal c axis

P. D. Horn and Y. M. Gupta
Shock Dynamics Laboratory, Department of Physics, Washington State University, Pullman, Washington 99164-2814
(Received 9 May 1988)

The ruby luminescence R-line spectrum has been measured under shock wave, uniaxial strain compression along the crystal c axis. Because the compression is elastic for the stress range reported here, changes in the R-line spectrum are reversible upon unloading. The magnitude of the wavelength shift for the R lines under shock loading is comparable to that observed in hydrostatic loading, but there are measurable differences: the present data show a nonlinear change with density compression; the R_1-R_2 splitting decreases with increasing compression. The shock data, despite the strongly nonhydrostatic state of stress in the ruby, show no broadening of the R lines. A discussion of the observed behavior, under uniaxial strain, in terms of the point-charge ligand-field model is presented.

I. INTRODUCTION

Spectroscopic studies of impurity ions in crystals provide insight into the nature of the local environment around impurity sites.[1] As an example, a number of theoretical and experimental studies have been carried out on ruby crystals to develop a detailed understanding of the spectra of Cr^{3+} ions in the host Al_2O_3 lattice in terms of crystal-field theory.[2,3] Although stress-induced changes in the optical spectra of ruby are expected to be helpful in checking and/or refining the theoretical calculations, previous studies[4–6] have met with limited success due to the complex strain states involved. It would be particularly desirable to examine the sharp emission lines with the samples subjected to well-defined and simple strain states along different crystallographic directions. Shock-wave experiments, although inherently difficult, are attractive for meeting these needs. In addition, the study of impurity-ion spectra under shock loading opens up the possibility of using the optical spectra as an atomic probe of shock-induced changes in solids.

We have recently demonstrated the feasibility of making time-resolved measurements of the ruby-luminescence R lines during shock compression.[7] However, the quality of the data did not permit accurate quantitative measurements. Since then the experimental method has been modified considerably to permit quantitative measurements of the R-line wavelength shifts reported here.

Ruby is well suited for the present work because of its strong, sharp emission lines (R lines), the fact that Cr^{3+} substitutes for Al^{3+} without charge-compensating defects, and the availability of high-quality crystals. The R-line luminescence spectrum consists of two sharp lines (R_1,R_2) whose mean energy is determined mainly by the Coulomb interaction among the $3d^3$ valence electrons of Cr^{3+} as modified by the crystal field associated with the six nearest-neighbor oxygen ions. The R_1-R_2 splitting results from spin-orbit coupling in the presence of the trigonal field due to these oxygen ions.[1]

At ambient conditions, the R lines lie at 6943 Å (R_1) and 6929 Å (R_2).[6] The wavelength shift of the R_1 line has been studied under static high pressure and is routinely used for pressure calibration into the Mbar range.[8–11] Because the wavelength-shift–pressure relationship in the ruby is determined using the response of other materials,[8] the ruby calibration is often termed as a secondary pressure scale. Munro *et al.* have presented a good compilation of hydrostatic results and temperature effects.[12] Under hydrostatic pressure, the two R lines shift equally and no change in the R_1-R_2 splitting occurs.

A quantitative measurement of the wavelength shift of the R lines under shock loading is also expected to be valuable in relating pressure (or stress) measurements between shock[13–15] and static high-pressure data. In shock-wave experiments, both the density change and longitudinal stress in the ruby can be determined directly with considerable accuracy as discussed in a later section. Hence, the shock experiments provide a method for directly relating the R-line shift to a well-characterized state of stress and strain in the ruby.

II. EXPERIMENTAL METHOD

The experimental arrangement is shown in Fig. 1. Shock waves were generated by impacting the samples with sapphire plates, which were mounted on projectiles and accelerated to desired velocities using a compressed gas gun. Longitudinal stresses in the range 20–125 kbar were achieved with impact velocities ranging from 200 to 600 m/s. The sample assembly will be discussed in detail after the overall apparatus is described.

Luminescence was excited with light from a cw argon laser (5145 Å, Coherent Innova 90-6), which was transmitted to the sample by an optical fiber (Diaguide SMY 400UV). The same fiber was used to collect the luminescence and deliver it to the recording system, which was by necessity located away from the target area. This luminescence was then collimated, separated from the laser path by a dichroic beam splitter, and focused into a double spectrograph [Spex 1680 with 1200-

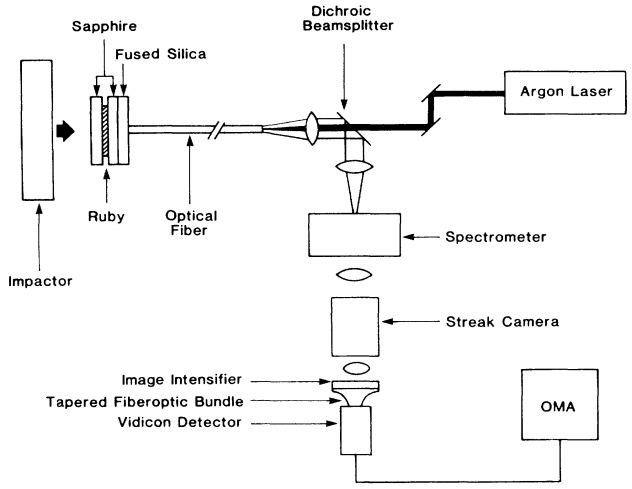

FIG. 1. Schematic view of overall experimental arrangement. The thickness of the ruby sample is exaggerated in this figure.

(groove/mm) gratings and silver-coated mirrors]. The luminescence spectrum was dispersed over time by an image-converter streak camera (Cordin model 160). The streak image was focused onto a microchannel-plate image intensifier (ITT model F4113P11), which in turn was coupled to a Vidicon detector by a tapered fiberoptic bundle. The Vidicon output was recorded by an optical multichannel analyzer (EG&G OMAIII with model 1254 Vidicon detector). During the shock experiment, the spectrum was recorded 50 times at 30-ns intervals. The streak camera and the image intensifier were triggered at the appropriate time by shorting a charged trigger pin, mounted at a specified height above the impact surface, with the projectile.

The ruby samples, obtained from Crystal Optics Research, were z-cut disks 19 mm in diameter and 0.13–0.26 mm thick, and contained 0.5% Cr_2O_3 by weight. Thin disks were used so that the transit time of the shock across the ruby (12–24 ns) would not limit the time resolution. The time resolution for the system, in the experiments reported here, was approximately 30 ns. This resolution, if needed, can be reduced to ≈ 10 ns. A thin layer of aluminum was vapor deposited on the impact side of the ruby to enhance both the generation and collection of luminescence. The other components of the target were two z-cut sapphire (Adolph Meller Co.) disks and one fused-silica disk (Dynasil 1000) that were 25.4 mm in diameter and 3.2 mm thick. The disks were pressed together in the configuration shown in Fig. 1 with all contact surfaces being first coated by a vapor-deposited layer of indium, and were then potted into an aluminum target ring with epoxy. The indium served to keep epoxy from creeping between disks during potting in the target ring. A small area in the center of the ruby, rear sapphire, and fused silica was kept clear of indium for the passage of laser light and luminescence.

The purpose of the fused-silica disk at the back of the target was to provide a second data point in each experiment when the stress at the ruby was relieved by a rarefaction generated at the sapphire-silica interface.[16] The impactors in all of the experiments were also z-cut sapphire disks (50.8-mm diameter, 6.4 mm thick). By maintaining the z-cut crystal orientation, we avoided mismatches of mechanical impedance at the sapphire-sapphire and sapphire-ruby interfaces. Throughout this paper we will assume that the mechanical properties of ruby and sapphire are the same. Based on existing data, this is an excellent assumption in the elastic range.

A wavelength calibration of the recording system was performed prior to each experiment. Because no independent calibration sources were available for the narrow spectral range observed (approximately 6890–6990 Å), the ruby R_1 and R_2 lines themselves were used. The R-line positions were recorded at several settings of the spectrograph wavelength selector with the streak camera in the focus mode. The system dispersion proved to be linear over this range, and its value was obtained from a least-squares fit. A streak record of the ambient spectrum was also recorded prior to each experiment, and wavelength shifts were determined with respect to that reference. During the experiment, the laser beam was blocked until a few seconds before the shock event to avoid heating the sample. We believe this to be sufficient due to the high thermal conductivity and large thermal mass of the sapphire disks that are in contact with the ruby samples.

III. RESULTS

A typical output from the optical multichannel analyzer displaying an intensity-time-wavelength plot is presented in Fig. 2; 24 of the 50 spectra recorded over time in a 100-kbar experiment are shown. The first five spectra in Fig. 2 were obtained before the arrival of the shock wave at the ruby sample. Spectra 6–14 were recorded after the ruby sample was shocked and during the period of constant stress (100 kbar) in which the shock wave traveled to the sapphire–fused-silica interface and a rarefaction wave from this interface traveled back to the ruby. The rarefaction wave resulted in partial unloading in the ruby to approximately 42 kbar and spectra 15–19 correspond to this stress value. After this,

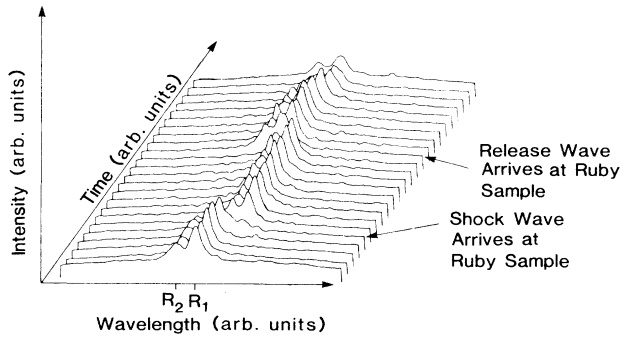

FIG. 2. Intensity-wavelength-time plot of the R-line spectrum for a 100 kbar shock experiment. The spectra in this figure are separated by 30-ns intervals.

relief waves from the sample edges arrived in the central area of the sample from which luminescence is collected, and later data cannot be interpreted. Figure 3 is a comparison of one spectrum taken from Fig. 2 with the reference spectrum obtained at the same location on the detector prior to the shot, and the red shift of the R lines can be clearly observed. Spectra are always compared from the same location on the detector screen to avoid any effects of image distortion or misalignment of the detector axes with respect to the time and wavelength axes of the streak camera. The spectra in both Figs. 2 and 3 have been digitally smoothed over approximately 1.6 Å by use of a sliding average. Detailed examination of the data in Fig. 3 show two interesting results that are discussed in the next section: there is no apparent broadening of the R lines despite the strongly nonhydrostatic state of stress present in the shock experiments; the R_1-R_2 splitting is decreased in the shocked state.

The centroids of the R-line peaks were located to within ± 1 Å and the wavelength shifts for a given spectrum were determined. The wavelength-shift values from four or five spectra at a given stress were then averaged to give the $\Delta\lambda$ values for that stress. The statistical error of the mean should, therefore, be approximately ± 0.5 Å. The results from all of our experiments are summarized in Table I. As indicated earlier, we have assumed that the thermomechanical properties of the ruby and sapphire are identical in the range of elastic compression. The particle velocities on impact are equal to half the projectile velocity[15] because these were symmetric impact experiments (sapphire on sapphire). The rarefaction from the sapphire–fused-silica interface results in an increase in the particle velocity in the ruby. The shock response of z-cut sapphire has been carefully examined by Barker and Hollenbach[16] to 120 kbar. These authors show that a linear shock-velocity–particle-velocity relation provides an excellent fit to their data.

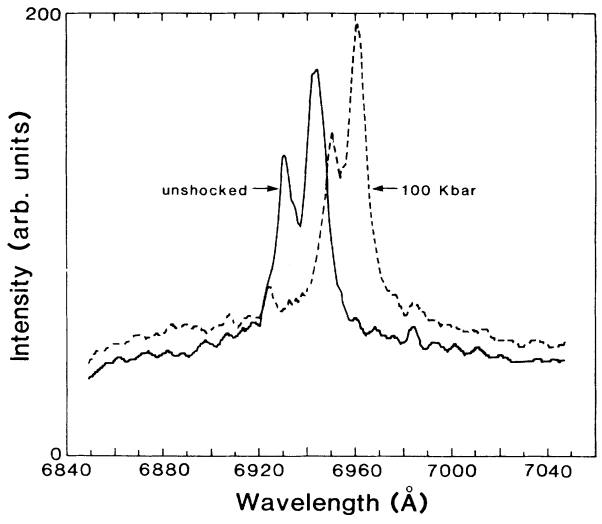

FIG. 3. Ruby R-line spectrum at 100 kbar and at ambient conditions.

TABLE I. Compilation of ruby-luminescence data from shock-wave uniaxial-strain experiments.

Experiment number[a]	Particle velocity[b] (mm/μs)	Density compression[c]	Longitudinal stress[c] (kbar)	Longitudinal stress[d] (kbar)	Lateral stress[d] (kbar)	$\Delta\lambda_{R_1}$ (Å)	$\Delta\lambda_{R_2}$ (Å)	ΔT (K)	$\Delta\lambda_{R_1}$ corrected (Å)	$\Delta\lambda_{R_2}$ corrected (Å)
1	0.111	0.0099	50.0	49.9	11.4	7.4	9.1	3.5	7.2	8.9
1_r	0.175	0.0042	21.0	21.0	4.7	2.9	4.1	1.5	2.8	4.0
2	0.166	0.0148	75.1	74.9	17.3	12.3	14.2	5.4	12.0	13.9
2_r	0.263	0.0062	31.0	30.9	7.0	4.5	5.8	2.3	4.4	5.7
3	0.220	0.0197	100.0	99.5	23.3	17.2	20.0	7.2	16.8	19.6
4	0.222	0.0198	101.0	100.4	23.5	16.7	19.3	7.4	16.3	18.9
5	0.272	0.0243	124.2	123.4	29.2	22.3	25.3	9.0	21.8	24.8
5_r	0.433	0.0099	50.0	49.9	11.4	7.8	9.2	3.7	7.6	9.0

[a]Subscript r on experiment number indicates relief data.
[b]The particle velocity is merely half the projectile velocity measured in the experiments.
[c]Obtained from the data of Barker and Hollenbach (Ref. 16) on z-cut sapphire. These data do not provide information about lateral stresses.
[d]Calculated using the nonlinear elastic constants from the work of Hankley and Schuele (Ref 17).

$$D = 11.19 + 1.0u \text{ mm}/\mu\text{s} , \quad (1)$$

where 11.19 is the ultrasonic wave velocity measured at ambient conditions. This value is in good agreement with the ultrasonic results of Hankley and Schuele.[17] The above relation, in conjunction with the Rankine-Hugoniot relations[15]

$$\frac{\rho}{\rho_0} = \frac{D}{D-u} , \quad (2)$$

$$\sigma_{33} = \rho_0 D u , \quad (3)$$

was used to obtain the density compression ($\mu \equiv \rho/\rho_0 - 1$) and the longitudinal stress in Table I. Because the Rankine-Hugoniot relations do not provide the lateral stresses ($\sigma_{11} = \sigma_{22}$), nonlinear elastic relations, described in the Appendix, were also used to obtain the longitudinal and lateral stresses. Excellent agreement can be seen between the longitudinal stress values calculated from Barker and Hollenbach's results and those obtained from the nonlinear elastic response. For a stiff material like sapphire, at these compressions, this agreement is not very surprising.

Over the stress range of our experiments, both the shock and release states can be treated as isentropic and the temperature change can be expressed as

$$\Delta T = T_0(e^{(\gamma/V)\Delta V} - 1) , \quad (4)$$

where γ is the Grüneisen parameter and V is the specific volume. We have used a value[18] of $\gamma = 1.27$ and $V_0 = 0.251$ cm^3/g, and assumed that γ/V has a constant value of 5.06 g/cm^3. The calculated temperature changes are less than 10 K in all cases and, hence, the wavelength-shift corrections ($0.06\,\Delta T$) due to temperature[12] are smaller than the experimental precision. Nevertheless, they have been included here for completeness. Barker and Hollenbach[16] have estimated the temperature increase of z-cut sapphire shocked to 117 kbar to be 40 K; no explanation was given regarding the method used to obtain this value. We believe that the 40-K value is too high.

IV. ANALYSIS AND DISCUSSION

The wavelength shifts of both the R_1 and R_2 lines are plotted as a function of density compression in Fig. 4. Although the longitudinal stress scale (pertinent only to the shock data) is shown at the top of the figure, choice of density compression facilitates comparison with hydrostatic data. The wavelength shifts of the R_1 and R_2 lines were fitted using a least-squares analysis,

$$\Delta\lambda = a\mu + b\mu^2 ,$$

where $a = 650$ Å and $b = 10\,000$ Å for the R_1 line and $a = 850$ Å and $b = 6900$ Å for the R_2 line. The uncertainties in the a and b parameters are estimated to be 10% and 25%, respectively. The corresponding change in $\Delta\lambda$ is less than 0.5 Å in this range of compression. The ± 0.5-Å statistical error of these data is indicated by the size of the data-point symbols in the figure. The agreement between loading and unloading data indicates that the ruby and sapphire behave elastically in this range of stress. Because of the anticipated inelastic deformation of the ruby at higher stresses, we recommend against using the fits presented here to higher compressions in shock-wave studies. Experiments at higher stresses are currently under way. The dashed curve in Fig. 4 was calculated using the wavelength shift measured under hydrostatic compression:[12] 0.366 Å/kbar. The pressure-density relation for hydrostatic loading was obtained using a bulk modulus[19] of 2.544 Mbar and a pressure derivative of the bulk modulus[19] as 4.275. This effectively amounts to the use of a Murnaghan equation.

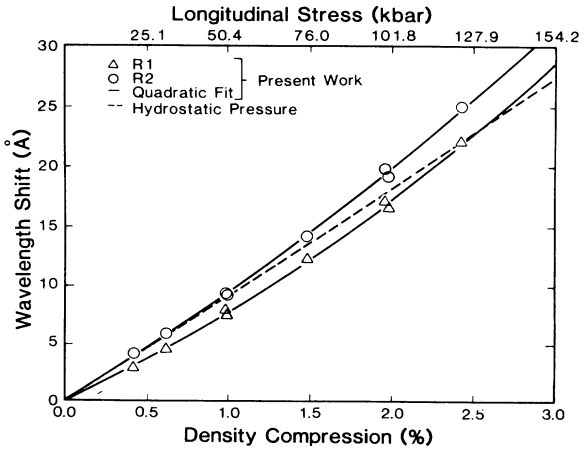

FIG. 4. Wavelength shift of R_1 and R_2 lines as a function of density compression. The ± 0.5-Å statistical error of these data are indicated by the size of the symbols used to denote the measured values. The dashed line represents the wavelength shift of both R_1 and R_2 lines under hydrostatic loading (Ref. 12).

As seen in Fig. 4, the wavelength shifts for different states of stress are different for the same density compression, i.e., volume alone is insufficient to define the ruby shift(s). The shock-wave results show a nonlinear change and the two R lines do not shift equally with compression in shock-wave studies. The R_1-R_2 splitting as a function of density compression is presented in Fig. 5. The results

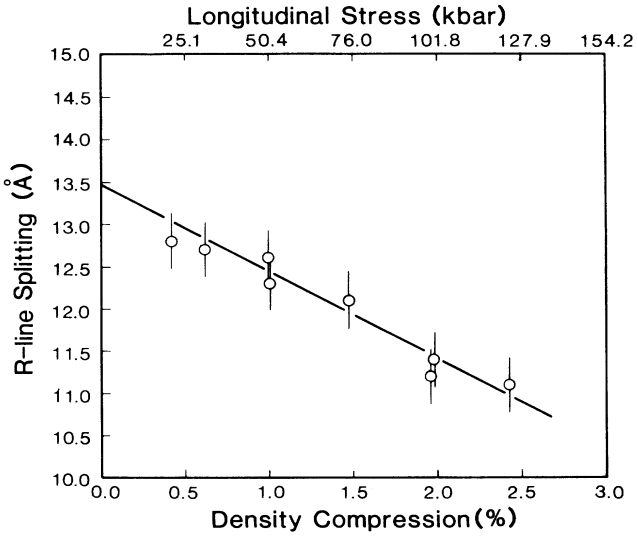

FIG. 5. R_1-R_2 splitting as a function of density compression.

can be fitted quite well to a straight line:

$$\Delta_{R_1\text{-}R_2} = 13.5 - 104\mu \text{ Å} .$$

The statistical error in these values is ±0.7 Å (from the ±0.5-Å variations in R_1 and R_2). The ambient-state intercept of this fit, 13.5 Å, falls below the expected value of 14 Å. This difference is also seen in the data during the ambient portion of some experimental records, and may be due to a small systematic bias in choosing the peak positions because of the overlap of the R_1 and R_2 spectra at room temperature and for the given spectrometer resolution. Because of this overlap, the apparent positions of the peaks could be shifted toward their mutual center. This would essentially displace the entire curve of Fig. 3, but would have little effect on measurements of the wavelength shift of R_1 or R_2. The shift is determined from the difference between a shock spectrum and a reference spectrum, both of which are subject to nearly the same overlap bias; hence, the effect of the bias is canceled when the difference is taken.

Rather than discussing the shifts of the R_1 and R_2 lines individually, we will consider the results in terms of an overall shift of both lines accompanied by a change in R_1-R_2 splitting. We may then more easily examine the relative effects of the physical phenomena responsible, i.e., changes in the Coulomb interaction of Cr^{3+} electrons and the coupled spin-orbit-interaction–trigonal distortion, within the framework of ligand-field theory. It is a widely accepted that the point-charge model is not adequate to fully describe the R-line spectrum.[1] It does, however, provide some insight into the qualitative changes observed. The R_1 and R_2 lines originate in states split from a degenerate ^2E_g term by the trigonal distortion and spin-orbit coupling. These states are of equal degeneracy (only Kramers degeneracy remains), so that the effect of the changing Coulomb interaction in this strong-field case ($H_{\text{ligand}} > H_{\text{Coulomb}} > H_{\text{spin orbit}}$) is simply to shift the average of the R_1 and R_2 energies. The wavelength-shift–density-compression plots in Fig. 4 show that the average of R_1 and R_2 line shifts is comparable to the hydrostatic result; the average value is less than the hydrostatic value up to 2% compression and is larger at higher compressions. It then seems reasonable to conclude that in the range of compression considered here, the change in Coulomb interaction is mainly a density effect with some perturbation related to the symmetry of the distortion. In the point-charge model, the R_1-R_2 splitting is proportional to the product of the trigonal distortion and spin-orbit coupling,[1] and is, therefore, more sensitive than the Coulomb interaction to the symmetry of the stress-induced distortion, e.g., compression along the trigonal axis as in the present experiments. As shown in Table I, the splitting is decreased by 21% under uniaxial strain at 2.4% density compression (124.2 kbar longitudinal stress). No change in R-line splitting is observed under hydrostatic loading for comparable compressions.[12] The dependence of these spectral changes on the symmetry of the distortion points out the need to consider not just the bulk strain, but the rearrangement of oxygen ions in the vicinity of the chromium ions. The chromium ion is an atomic inclusion in the Al_2O_3 lattice, and there is no reason to expect the local deformation to match that of the bulk. Efforts have been made to develop a phenomenological connection between bulk and local deformation,[20–23] based on their respective symmetries, under hydrostatic and uniaxial stress. That method yields only symmetry-labeled "strains" (displacements) summed over oxygen ions, and provides limited insight into the details of the local atomic environment. The ability to study the simpler uniaxial bulk strain in shock-wave experiments may prove a real advantage in the consideration of this problem. A more detailed understanding awaits further study.

In static high-pressure studies, broadening of the R lines is attributed to the ruby being subjected to nonhydrostatic stress.[12] In the shock experiments reported here, the stress state in the ruby is strongly nonhydrostatic (see Table I) but uniform for times of interest and no broadening of the R lines is observed. This result suggests that line broadening (in the absence of temperature increase) in static high-pressure studies is due to nonuniformity of the stress in the ruby samples. A similar conclusion, using an empirical spectral line-shape model, was presented in Sec. IV of Ref. 12. In using the empirical model, these authors assume the state of stress in the ruby to be locally hydrostatic but nonuniform; the superposition results in a broad distribution of pressure in the ruby sample which causes line broadening. We believe that the stress state in the ruby sample in both nonuniform and nonhydrostatic. The latter, however, is not the cause of line broadening as indicated by our results. Extensive broadening of the spectra from a single ruby chip in static measurements indicates a substantial nonuniformity of stress over the dimension of the ruby chip making it difficult to attribute a single mean stress (or pressure) value to even small regions of the ruby.

V. CONCLUSION

Quantitative measurements of the wavelength shift of the ruby R lines under uniaxial strain along the crystal c axis have been obtained to 125 kbar longitudinal stress. Over this stress range the ruby is elastic, the thermal effects are negligible, and the stresses in the ruby can be accurately determined. The principal uncertainty in our data is in the spectral resolution (0.5 Å). Despite the strongly nonhydrostatic state of stress in the shocked ruby, the results show no broadening of the R lines. This suggests that line broadening observed in static high-pressure studies is caused by nonuniform stresses. The magnitude of the R-line wavelength shifts, comparable to the shifts observed in hydrostatic measurements, can be attributed to compression-induced changes in the Coulomb interaction of the $3d$ chromium electrons. There are, however, two significant differences in comparison to the hydrostatic results: the wavelength shift as a function of density compression is nonlinear and the R_1-R_2 splitting decreases with compression. This latter result would indicate a decrease in the product of spin-orbit coupling and the trigonal field under uniaxial compression along the crystal c axis.

The present work represents a start towards understanding changes in the ruby spectra for large and well-

defined compressions along different crystal axes. Studies are underway to examine the effects of temperature, crystal orientation, and inelastic deformation on both absorption and emission spectra.

ACKNOWLEDGMENTS

Dr. Michael Frankel of the U.S. Defense Nuclear Agency is acknowledged for his encouragement and support during the early stages of our work. Within our laboratory, Jim Burt, Jerry Thompson, and Paul Bellamy are thanked for their assistance with the experimental effort. Discussions with Jim Burt and Dr. S. M. Sharma regarding the theoretical work on the ruby spectra have been very beneficial to the authors. This work was supported by the Defense Nuclear Agency under Contract No. 001-85-C-0154.

APPENDIX: NONLINEAR ELASTIC RELATION FOR UNIAXIAL-STRAIN COMPRESSION

The procedure used to determine the nonlinear elastic relations for the ruby and the sapphire for uniaxial-strain compression along the crystal c axis is described here. Our derivation is based on the finite-strain formulation presented by Thurston.[24,25] For the problem at hand, entropy changes due to shock compression are negligible. The initial and current configuration of a particle is denoted by a_i and x_i, respectively. The displacement and particle velocity are defined as

$$\alpha_i = x_i - a_i \ , \tag{A1}$$

$$u_i = \left[\frac{\partial x_i}{\partial t} \right]_a \ . \tag{A2}$$

A suitable measure of finite strain is the Green strain defined as[24]

$$\eta_{ij} = \frac{1}{2} \left[\frac{\partial x_m}{\partial a_i} \frac{\partial x_m}{\partial a_j} - \delta_{ij} \right] \ , \tag{A3}$$

where the Einstein summation convention is used. For uniaxial strain along the c axis, only η_{33} is nonzero. Using (A1) and (A3), we can write

$$\eta_{33} = \frac{\partial \alpha_3}{\partial a_3} + \frac{1}{2} \left[\frac{\partial \alpha_3}{\partial a_3} \right]^2 \ . \tag{A4}$$

To obtain the stress-strain relation, we consider a series expansion of the internal energy at constant entropy:

$$\rho_0 U(\eta_{ij},S) = \rho_0 U(0,S) + \tfrac{1}{2} C^S_{ijkl} \eta_{ij} \eta_{kl} + \tfrac{1}{6} C^S_{ijklmn} \eta_{ij} \eta_{kl} \eta_{mn} + \cdots \ , \tag{A5}$$

where U is the internal energy per unit mass and S is the entropy per unit mass. The isentropic elastic constants are defined by

$$C^S_{ijkl} = \rho_0 \left[\frac{\partial^2 U}{\partial \eta_{ij} \, \partial \eta_{kl}} \right]_S \ , \tag{A6}$$

and correspondingly for C^S_{ijklmn}. The thermodynamic stresses, referred to as the symmetric Piola-Kirchoff stresses, are given by[24]

$$t_{ij} = \rho_0 \left[\frac{\partial U}{\partial \eta_{ij}} \right]_S \ . \tag{A7}$$

Applying this to the series expansion in (A5), we obtain the relation between the thermodynamic stresses and the strain as

$$t_{ij} = C^S_{ijkl} \eta_{kl} + \tfrac{1}{2} C^S_{ijklmn} \eta_{kl} \eta_{mn} \ . \tag{A8}$$

Using the uniaxial-strain condition, we obtain

$$t_{ij} = C^S_{ij33} \eta_{33} + \tfrac{1}{2} C^S_{ij3333} \eta^2_{33} \ . \tag{A9}$$

For the present work, it is more convenient to express the stress-strain relations in terms of the Cauchy stresses defined by[24]

$$\sigma_{km} = \frac{1}{J} \frac{\partial x_k}{\partial a_j} \frac{\partial x_m}{\partial a_i} t_{ij} \ , \tag{A10}$$

where J is the Jacobian for the transformation between the two coordinate systems. For the one-dimensional case of interest, J takes a simple form (ρ_0/ρ).

The longitudinal (σ_{33}) and lateral $(\sigma_{11}, \sigma_{22})$ stresses can be written as

$$\sigma_{11} = \frac{\rho}{\rho_0} (C^S_{1133} \eta_{33} + \tfrac{1}{2} C^S_{113333} \eta^2_{33}) \ ,$$

$$\sigma_{22} = \frac{\rho}{\rho_0} (C^S_{2233} \eta_{33} + \tfrac{1}{2} C^S_{223333} \eta^2_{33}) \ , \tag{A11}$$

$$\sigma_{33} = \frac{\rho_0}{\rho} (C^S_{3333} \eta_{33} + \tfrac{1}{2} C^S_{333333} \eta^2_{33}) \ .$$

The value of C^S_{3333} can be calculated from the density $(\rho_0 = 3.985 \ \text{g/cm}^3)$ and longitudinal sound speed $(c_l = 11.19 \ \text{mm}/\mu\text{s})$ as $C^S_{3333} = 4990$ kbar. The remaining constants are given by Hankley and Schuele[17] as

$$C^S_{1133} = C^S_{2233} = 1109 \ \text{kbar} \ ,$$

$$C^S_{333333} = -33{,}400 \ \text{kbar} \ ,$$

and

$$C^S_{113333} = C^S_{223333} = -9220 \ \text{kbar} \ .$$

In analyzing the experimental data, the longitudinal stresses (along the c axis) were calculated from Barker and Hollenbach's shock data on z-cut sapphire. A seen in Table I, these values are in good agreement with the values calculated using the nonlinear elastic constants indicated above.[17] The corresponding lateral stresses were also obtained from Eq. (A11). For our work it is convenient to consider the stresses positive in compression; this convention is used in Table I.

In analyzing the shock data, it is convenient to use an engineering strain defined by

$$e = \frac{u}{D} = 1 - \frac{\rho_0}{\rho} \ , \tag{A12}$$

where u and D are particle and shock velocities, respec-

tively. For the present problem,

$$J=\frac{\partial x_3}{\partial a_3}=\frac{\rho_0}{\rho}=1+\frac{\partial \alpha_3}{\partial a_3} \ . \tag{A13}$$

Equations (A4), (A12), and (A13) can be combined to give

$$\eta_{33}=-e+\tfrac{1}{2}e^2 \ . \tag{A14}$$

The negative sign indicates here the usual convention of denoting η_{ij} positive in tension, whereas e in Eq. (A12) was defined to be positive in compression.

[1]S. Sugano, Y. Tanabe, and H. Kamimura, *Multiplets of Transition-Metal Ions in Crystals* (Academic, New York, 1970).

[2]Donald S. McClure, J. Chem. Phys. **36**, 2757 (1962).

[3]R. M. Macfarlane, Phys. Rev. **158**, 158 (1967).

[4]D. R. Stephens and H. G. Drickamer, J. Chem. Phys. **35**, 427 (1961).

[5]T. Goto, T. J. Ahrens, and G. R. Rossman, Phys. Chem. Miner. **4**, 253 (1979).

[6]A. L. Schawlow, in *Advances in Quantum Electronics*, edited by T. R. Singer (Columbia University Press, New York, 1961), p. 50.

[7]P. D. Horn and Y. M. Gupta, Appl. Phys. Lett. **49**, 856 (1986).

[8]Richard A. Forman, Gaspar J. Piermarini, J. Dean Barnett, and Stanley Block, Science **176**, 24 (1972).

[9]G. J. Piermarini, S. Block, J. D. Barnett, and R. A. Forman, J. Appl. Phys. **46**, 2774 (1975).

[10]D. M. Adams, R. Appleby, and S. K. Sharma, J. Phys. E **9**, 1140 (1976).

[11]H. K. Mao, P. M. Bell, J. W. Shaner, and D. J. Steinberg, J. Appl. Phys. **49**, 3276 (1978).

[12]R. G. Munro, G. J. Piermarini, and S. Block, J. Appl. Phys. **57**, 165 (1985).

[13]G. E. Duvall, in *Dynamic Response of Materials to Intense Impulsive Loading*, edited by P. C. Chou and A. K. Hopkins (Air Force Materials Laboratory, Wright Patterson AFB, Ohio, 1972), p. 89.

[14]Y. M. Gupta, in *Encyclopedia of Physics*, 3rd ed., edited by Robert M. Bescanon (Van Nostrand/Reinhold Co. New York, 1985), p. 1109.

[15]Lee Davison and R. A. Graham, Phys. Rep. **55**, 257 (1979).

[16]L. M. Barker and R. E. Hollenbach, J. Appl. Phys. **41**, 4208 (1970).

[17]Robert E. Hankley and Donald E. Schuele, J. Acoust. Soc. Am. **48**, 190 (1970).

[18]J. H. Gieske, Ph.D. thesis, Pennsylvania State University, 1968.

[19]H. d'Amour, D. Schiferl, W. Denner, Heinz Schulz, and W. B. Holzapfel, J. Appl. Phys. **49**, 4411 (1978).

[29]E. Duval, R. Louat, and R. Lacroix, Phys. Status Solidi **50**, 627 (1972).

[21]R. Lacroix, E. Duval, B. Champagnon, and R. Louat, Phys. Status Solidi **68**, 473 (1975).

[22]B. Champagnon and E. Duval, J. Phys. C **13**, 131 (1980).

[23]E. Duval, B. Champagnon, and R. Lacroix, J. Phys. C **13**, L147 (1980).

[24]R. N. Thurston, in *Physical Acoustics, Vol. I*, edited by W. P. Mason (Academic, New York, 1964).

[25]R. N. Thurston, in *Handbuch Der Physiks, Vol. VIA/4*, edited by C. Truesdall (Springer-Verlag, Berlin, 1974).